TASK QUARTERLY 8 No 4, 603–611

A NUMERICAL SOLUTION OF THE POISSON-SCHRÖDINGER PROBLEM FOR A VERTICAL GATED QUANTUM DOT

KRZYSZTOF LIS, STANISŁAW BEDNAREK
AND JANUSZ ADAMOWSKI

Faculty of Physics and Nuclear Techniques,
AGH University of Science and Technology,
Al. Mickiewicza 30, 30-059 Cracow, Poland
lis@fatcat.ftj.agh.edu.pl

(Received 6 June 2004)

Abstract: We present a numerical solution of the Poisson-Schrödinger problem for a semiconductor nanostructure containing a single quantum dot. The main outcome of our work is the lateral confinement potential, which determines the electronic properties of the nanodevice. We study the real nanodevice with cylindrical symmetry, which allows us to solve the three-dimensional problem on a two-dimensional mesh. We discuss the self-consistency of the solution with respect to the distribution of ionized donors inside the nanodevice.

Keywords: semiconductor quantum dots, quantum dots, Poisson-Schrödinger problem

1. Introduction

Enormous progress in electronics of the last few years mainly results from miniaturization of electronic circuits. It is expected that within the next few years miniaturization of electronic devices will achieve the regime in which quantum effects occur to their full extent. Therefore, it is necessary to include quantum effects into the study of sub-micrometer electronic devices. Quantum effects are dominant in nanometer-sized quantum dots (QDs) [1]. QDs are often called artificial atoms [2], as in a QD, similarly as in a natural atom, electrons confined in an external potential form discrete energy levels. The confining potential determines the electronic properties of the QD, such as the number of localized electrons (quantum capacity) and the energy spectrum. The confinement potential can be formed by a system of barriers created by the use of two kinds of materials. Such potential is build-in and cannot be altered after the QD's fabrication. The confinement potential can also be formed by external voltages applied to electrodes attached to the nanodevice. Tuning the electrostatic potential created by the electrodes makes it possible to control QD properties [3–5]. In most of the theoretical papers on QD's, a model potential is used in order to approximate the real confinement potential. Model confinement potentials are usually

in the form of rectangular wells or harmonic potentials and lead to a qualitative description of QDs only. In the present paper, we discuss a nanodevice [6–9] for which it is possible to calculate confinement potential from the first principles of electrostatics.

A schema of the nanodevice, which was constructed and studied by Ashoori *et al.* [6–9], is shown in Figure 1a. The nanodevice was build on the basis of a planar structure consisting of doped and undoped GaAs and AlGaAs layers. The bottom electrode is formed by a GaAs substrate layer heavily doped with donors. The following sequence of layers was grown on the substrate: a 60 nm GaAs spacer layer, a 12.5 nm AlGaAs tunnel barrier, a 17.5 nm GaAs quantum well, in which the electrons are localized, and a 50 nm AlGaAs blocking layer. This blocking layer consists of two parts: a 15 nm undoped layer, which adheres to the quantum-well layer, and a 35 nm donor-doped layer. Above the blocking layer, there is a GaAs cap of 30 nm height and diameter ranging from 300 nm to 1500 nm. The entire nanostrucure is covered with metal, which forms the top gate.

Throughout the present paper, we consider a nanostructure with a cap of the diameter of 1100 nm. Voltage, V_g, applied between the bottom and top electrodes generates an electrostatic field inside the nanodevice. The cap of the nanodevice [6–9] produces the inhomogeneity of the electrostatic field which is the source of lateral confinement, *i.e.* confinement of electrons in the $x-y$ plane. The confinement in the vertical (z) direction results from band offset (*cf.* Figure 1b). The depth of the corresponding potential well is ~ 0.2 eV.

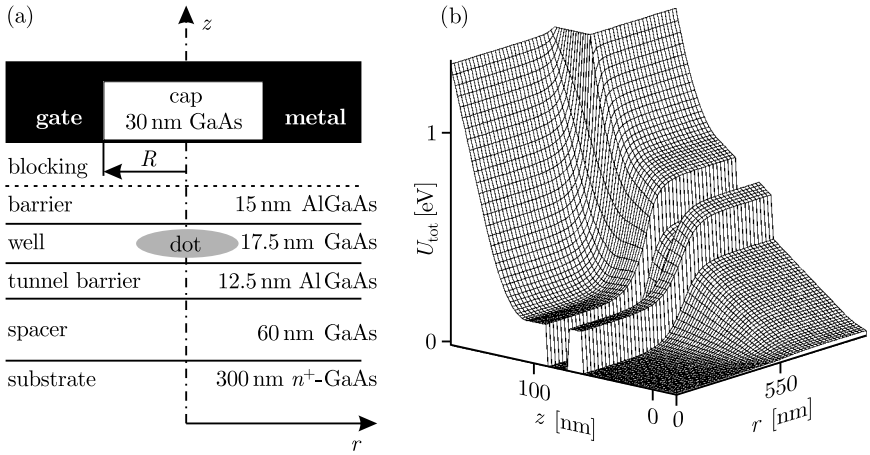

Figure 1. (a) A schema of the model nanodevice; the center of the cylindrical coordinate system is at the substrate-spacer interface; (b) the total potential energy $U_{\rm tot}$ of an electron as a function of cylindrical coordinates r and z

2. Model

The electrostatic potential depends on the voltage applied to the gate, the geometry of the nanodevice, the ionized donor distribution, the charge induced on the metallic gate, and the charge of electrons confined in the QD. We calculate

the electrostatic confinement potential by solving the Poisson-Schrödinger problem, which is composed of two parts. The charge density distribution of electrons localized in the QD is determined by their wave functions, which are the outcome of the quantum problem, while the electrostatic potential is calculated from the Poisson equation, *i.e.* from classical electrostatics. Potential φ_e generated by the electrons confined in the QD plays a different role than potential φ_b, which stems from other sources. Therefore, we use the superposition rule and separate the total electrostatic confinement potential, φ_{elst}, as follows:

$$\varphi_{\text{elst}} = \varphi_e + \varphi_b. \tag{1}$$

Potential φ_b confines the electrons and is substituted into the Schrödinger equation as a part of the external potential. The potential created by the QD-confined electrons can be approximated with a Hartree potential of the form:

$$\varphi_e(\mathbf{r}) = \frac{e}{4\pi\varepsilon\varepsilon_0}\int \frac{\rho_e(\mathbf{r}')}{|\mathbf{r}-\mathbf{r}'|}d\mathbf{r}', \tag{2}$$

where e is the elementary charge, ε is the dielectric constant of GaAs, and ρ_e is the charge density of the electrons confined in the QD.

The field generated by the ionized donor centers in the n-doped layers and by the surface charge on the metallic electrode was found by solving the Poisson equation in the cylindrical coordinates:

$$\left(\frac{\partial^2}{\partial r^2}+\frac{1}{r}\frac{\partial}{\partial r}+\frac{\partial^2}{\partial z^2}\right)\varphi_b(r,z) = -\frac{\rho_D(r,z)}{\varepsilon\varepsilon_0}, \tag{3}$$

where ρ_D is the charge density associated with the ionized donors. Since each donor ionization event results from the transfer of a single electron from the donor level to the conduction band's bottom, we assume that the Fermi-Dirac distribution can be applied to the ionized-donor charge density, which leads to:

$$\rho_D(r,z) = \frac{n_D}{1+\exp\left(\frac{e\varphi_{\text{elst}}(r,z)+E_D}{k_BT}\right)}, \tag{4}$$

where E_D is the donor ionization energy, k_B – the Boltzmann constant, T is the temperature, and n_D is the concentration of the donors.

At low temperatures (experiments [6–9] were performed at 0.1K), the distribution of the ionization events as a function of the electron energy is almost binary in character. A single donor becomes ionized if the potential energy the of electron bound to the donor, *i.e.* $-e\varphi_{\text{elst}}(r,z)$, exceeds the donor ionization energy. Thus, we obtain the following donor-ionization condition:

$$\rho_D(r,z) = \begin{cases} 0 & \text{if} \quad -e\varphi_{\text{elst}}(r,z) < E_D, \\ n_D & \text{if} \quad -e\varphi_{\text{elst}}(r,z) > E_D. \end{cases} \tag{5}$$

In the present paper, we have chosen the potential of the bottom electrode as the zero point of the electrostatic-potential scale.

The charge density of ionized donors is the source of one component of the electrostatic field and – according to condition (5) – depends on the total electrostatic field. Therefore, we have to use the self-consistent iterative method in order to solve the Poisson-Schrödinger problem. In the first step of the iteration procedure, we assume

the absence of charge in the QD. The calculations are performed until self-consistency is achieved. Unfortunately, this procedure is numerically unstable at low temperatures. We remove this instability by simulating the physical process of cooling the system, which allows us to achieve the convergence of the numerical method. We assume that cooling starts at a quite high temperature ($T \simeq 15\,\mathrm{K}$), which smooths the sharp boundaries of the ionization region (*cf.* Figure 2a). Next, we slowly decrease the temperature to 0.1K.

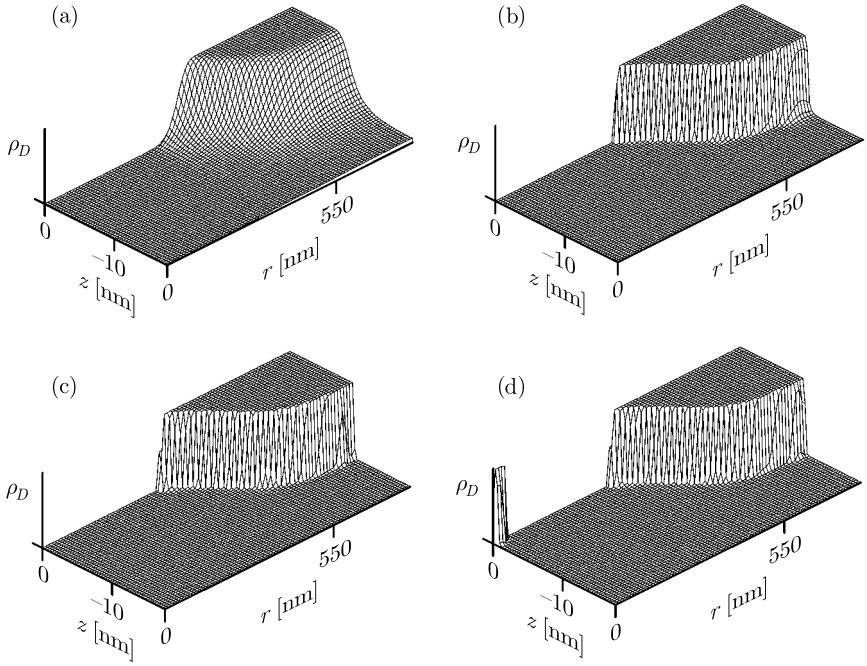

Figure 2. Spatial distribution of the ionized-donor charge density: (a) for $T = 15\,\mathrm{K}$ and an empty QD, (b) for $T = 0.1\,\mathrm{K}$ and an empty QD, (c) for $T = 0.1\,\mathrm{K}$ and a single electron localized in the QD, (d) for $T = 0.1\,\mathrm{K}$ and a single electron localized in the substrate layer

To solve the Poisson equation (3), boundary conditions need to be applied to potential φ_b on the surface enclosing the calculation domain. The boundary conditions can be conveniently determined for the total electrostatic potential, φ_{elst}. Potentials φ_b and φ_{elst} are identical if the QD is empty. If the QD contains electrons, we calculate the boundary values of φ_b from Equation (1). Since the nanostructure is cylindrically symmetrical, we apply the boundary conditions to the cylinder surface. On both (top and bottom) cylinder bases the boundary conditions are set by the voltages applied in the experiments [6–9]. At the metal-semiconductor interface, we additionally take into account the Schottky barrier, $\phi_B = 0.65\,\mathrm{V}$, and put $\varphi_{\mathrm{elst}} = V_g - \phi_B$ at the top gate. We place the bottom cylinder base deep into the substrate, where $\varphi_{\mathrm{elst}} = 0$. The radius of the cylinder is so large that the electric field on the side surface of the cylinder is approximately parallel to the z axis. In this case, the Poisson equation becomes one-dimensional and only voltage V_g is needed to determine $\varphi_{\mathrm{elst}}(z)$. Since both the electron charge and potential φ_b are negative, in Figure 3 we display

the electrostatic potential energy, U_b, of an electron instead of the electrostatic potential, *i.e.*:

$$U_b(r,z) = -e\varphi_b(r,z). \tag{6}$$

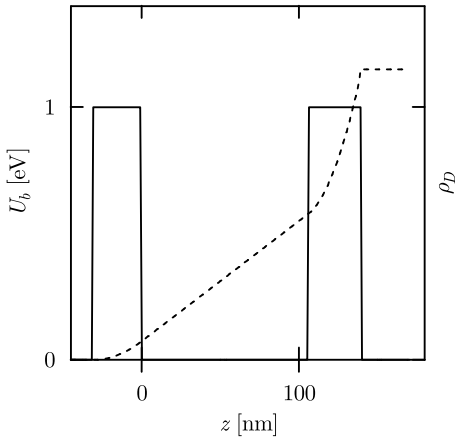

Figure 3. Electrostatic potential energy, U_b, of an electron (dashed line) and the charge density of ionized donors (solid line) as functions of z drawn at a distance from the cylinder axis

Figure 3 shows $U_b(z)$ which corresponds to the boundary condition on φ_b on the cylinder's side surface. We obtain a more appealing and clearer picture when displaying the total energy of the electron (*cf.* Figure 1b). Total potential energy U_{tot} is the sum of the electrostatic potential energy and the band offset energy. Band offsets are clearly visible in Figure 1b.

The Poisson equation (3) was solved numerically on a mesh. The system's symmetry allowed us to use a two-dimensional mesh. Potential $\varphi_b(r,z)$ was calculated using the relaxation method with a multigrid. In the inner part of the integration domain, the second derivative in Equation (3) was approximated by the five-point formula. We used three-point approximation only for the points at the boundary. When solving the Poisson equation along the symmetry axis we encountered divisions by 0 resulting from the second term on the left side of Equation (3). We removed this singularity by using the following property of the potential:

$$\left.\frac{\partial\varphi_b(r,z)}{\partial r}\right|_{r=0} = 0,$$

which results from the existence of a local extremum of the potential for $r = 0$. We interpolated the value of $\varphi_b(0,z)$ using a parabolic form:

$$\varphi_b(0,z) = \frac{1}{3}\left[4\varphi_b(\Delta,z) - \varphi_b(2\Delta,z)\right], \tag{7}$$

where Δ is the mesh step of the radial coordinate.

In Figure 1b, we display the total potential energy, $U_{\text{tot}}(r,z)$, calculated for the gate voltage of $V_g = -0.55\,\text{V}$ for an empty QD. If an electron is confined within the QD, we introduce U_{tot} into the Schrödinger equation as the external confinement

potential. For a single electron, the Schrödinger equation in the cylindrical coordinates has the following form:

$$-\frac{\hbar^2}{2m^*}\left(\frac{\partial^2}{\partial r^2}+\frac{1}{r}\frac{\partial}{\partial r}+\frac{l^2}{r^2}+\frac{\partial^2}{\partial z^2}\right)\Psi+U_{\mathrm{tot}}\Psi=E\Psi, \tag{8}$$

where l is the orbital-momentum quantum number, m^* is the effective band mass of the electron in GaAs, Ψ is its wave function, and E is its energy.

The Schrödinger equation (8) can be solved by the imaginary time method [10], which is described in the Appendix. The mesh used to solve Equation (8) in the r-coordinate is four times larger than that used in the Poisson equation (3). The electron wave function, obtained from Equation (8), is used to calculate the electron charge density according to:

$$\rho_e(\mathbf{r})=-e|\Psi(r,z)|^2. \tag{9}$$

This charge density is substituted into Equation (2) to calculate potential φ_e, which is then used to modify the boundary conditions for potential φ_b. When changing the boundary values of the total potential, we simultaneously change this potential in the entire domain of calculations. Therefore, this procedure is repeated until convergence is reached. The electron energy converges quickly, *viz.* in a dozen iterations. It is more difficult to obtain a stable distribution of the ionized donors at the real, *i.e.* very low temperature. We have solved this problem by introducing the simulated annealing method described above.

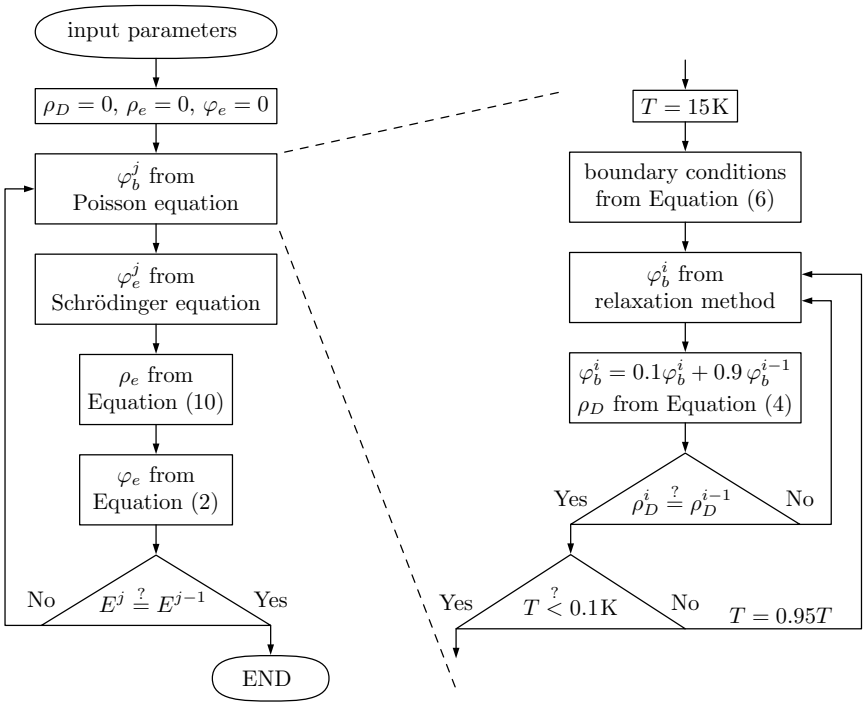

Figure 4. A block diagram of the self-consistent algorithm for a solution of the Poisson-Schrödinger problem

A block diagram of the algorithm is depicted in Figure 4. The main iteration loop is shown on the left side of this figure. The loop is terminated when self-consistency is reached between the electron charge density and the electron energy. The inner iteration loop, which ensures self-consistency between the ionized-donor charge density and the electrostatic field is shown on the right side of Figure 4.

3. Results and discussion

The temperature dependence of the ionized-donor distribution is shown in Figures 2a and 2b. For $T = 15\text{K}$ (*cf.* Figure 2a), we have obtained a smooth border between the charged and neutral regions of the substrate. However, this border becomes sharp for $T = 0.1\text{K}$ and the space-charge distribution function is binary in character (*cf.* Figure 2b). The distributions shown in Figures 2a and 2b have been obtained for an empty QD. These distributions lead to the electrostatic potential energy of contours shown in Figure 6a. We see that there exist two regions in the nanodevice with negative potential energy, in which the electron can be localized. The first region, with a deeper potential well, is located in the quantum-well layer (dark gray area in Figure 6a). The second region is wider and is located in the spacer layer (light gray area in Figure 6a).

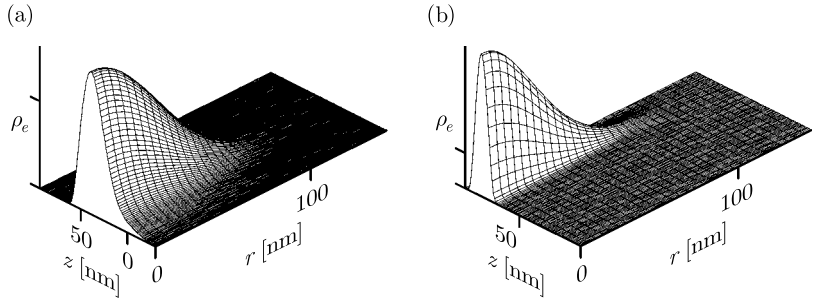

Figure 5. Electron charge density ρ as a function of cylindrical coordinates r and z for (a) an electron localized in the spacer, and (b) an electron localized in the quantum well

The presence of an electron in the QD changes both the potential φ_b and the distribution of ionized donors in the substrate. The charge density for the electron localized in the QD is shown in Figure 5b. In this case, the ionized-donor distribution changes only slightly (*cf.* Figure 2c). At the same time, an electron localized in the spacer with the charge density as shown in Figure 5a induces a small island of ionized donors in the near-axis area (*cf.* Figure 2d). In both cases, the presence of an electron entails a deepening of potential energy (*cf.* Figures 6b and 6c).

4. Summary

In the present paper, we have presented a method to solve the Poisson-Schrödinger problem for an electrostatic QD. We have shown how we can determine the profile of the electrostatic potential in the entire nanodevice and the charge density of electrons confined in the QD. The approach proposed in our paper is based on the iterative procedure, which allows us to obtain self-consistency between the electrostatic potential, the charge density of electrons localized in the QD and the

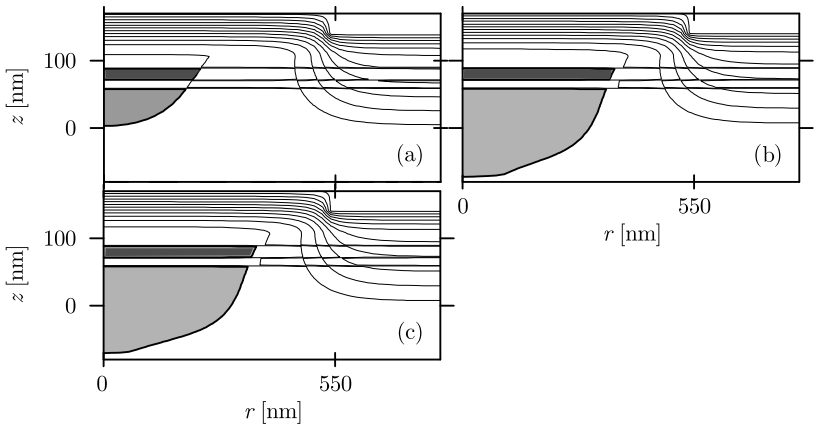

Figure 6. Contour lines of total potential energy U_{tot} of an electron as functions of cylindrical coordinates r and z. The regions of the electron's possible localization are marked light gray (the spacer layer) and dark gray (the quantum-well layer). The thick solid line corresponds to $U_{\mathrm{tot}} = 0$

distribution of ionized donors. We have found that the application of the simulated annealing method with the Fermi-Dirac distribution ensures convergence of the iterative procedure. This approach partly simulates the physical processes in the nanodevice. The most interesting physical outcome of the paper is the discovery of two distinct regions of the nanodevice in which electrons can be localized. Therefore, we obtain a double QD in a single-QD nanostructure. As a consequence, the distribution of ionized donors and the profile of the electrostatic potential depend on the region in which the electrons are actually localized.

5. Appendix: The imaginary time method

The imaginary time method is used to find stationary solutions to the Schrödinger equation [10]. This method is faster than the diagonalization methods and does not require putting the Hamiltonian into a matrix form. It can be used to solve eigenproblems on both two- and three-dimensional grids. Let us consider the time-dependent Schrödinger equation:

$$i\hbar\frac{\partial}{\partial t}\phi(r,t) = \hat{H}\phi(r,t), \tag{10}$$

where r denotes the set of spatial coordinates. If we replace in Equation (10) the real time variable t by an imaginary variable defined as $\tau = it\hbar$, we obtain:

$$\frac{\partial}{\partial \tau}\phi(r,\tau) = -\hat{H}\phi(r,\tau). \tag{11}$$

The formal solution of Equation (11) has the following form:

$$\phi(r,\tau) = \exp(-\hat{H}\tau)\phi(r,0). \tag{12}$$

An expansion of function $\phi(r,0)$ on the basis of the Hamiltonian eigenfunctions leads to:

$$\phi(r,\tau) = \exp(-\hat{H}\tau)\sum c_n\Psi_n(r) = \sum \exp(-E_n\tau)c_n\Psi_n(r). \tag{13}$$

In expansion (13), the terms corresponding to the excited states disappear exponentially with growing τ. For a large enough τ remains only the term which corresponds

to the ground state, Ψ_0, with the lowest energy, E_0. The eigenfunction and energy of the ground state can be obtained by the iteration procedure. In the initial step, we can generate the starting values of the ground-state wave function as random numbers. Next, we use them in the procedure:

$$\phi(r,\tau_i) = \phi(\tau_{i-1}) - \Delta\tau \hat{H}\phi(\tau_{i-1}), \tag{14}$$

until the convergence is reached. In the numerical version of Equation (14), we use finite-difference approximation for operator $\hat{H}$. Step $\Delta\tau$ cannot be too small to obtain convergence faster. At the same time, $\Delta\tau$ cannot exceed a critical value, since for too large $\Delta\tau$ the procedure becomes divergent. The average value of energy:

$$\langle\phi(r,\tau_i)|\hat{H}|\phi(r,\tau_{i-1})\rangle, \tag{15}$$

can be treated as a test parameter for convergence. After convergence is reached, the values of $\phi(r,\tau_i)$ are used as the ground-state wave function $\Psi_0(r)$.

Acknowledgements

The work has been partly supported by the Polish Scientific Research Committee (KBN).

References

[1] Jacak L, Hawrylak P and Wójs A 1998 *Quantum Dots*, Springer-Verlag, Berlin
[2] Maksym P A and Chakraborty T 1990 *Phys. Rev. Lett.* **65** 108
[3] Bednarek S, Szafran B and Adamowski J 2000 *Phys. Rev.* **B 61** 4461
[4] Bednarek S, Szafran B and Adamowski J 2001 *Phys. Rev.* **B 64** 195303
[5] Bednarek S, Szafran B, Lis K and Adamowski J 2003 *Phys. Rev.* **B 68** 155333
[6] Ashoori R C, Stormer H L, Weiner J S, Pfeiffer L N, Pearton S J, Baldwin K W and West K W 1992 *Phys. Rev. Lett.* **68** 3088
[7] Ashoori R C, Stormer H L, Weiner J S, Pfeiffer L N, Baldwin K W and West K W 1993 *Phys. Rev. Lett.* **71** 613
[8] Zhitenev N B, Brodsky M, Ashoori R C, Pfeiffer L N and West K W 1999 *Science* **285** 715
[9] Brodsky M, Zhitenev N B and Ashoori R C 2000 *Phys. Rev.* **B 61** 4718
[10] Davies K T R, Flocard H, Krieger S and Weiss M S 1980 *Nucl. Phys.* **111** 123